metals

Article

Microstructural Evolution and Subsequent Mechanical Properties of Ti65 Titanium Alloy during Long-Term Thermal Exposure

Juan Li [1], Wentao Jiang [2,*], Chunlin Xia [3], Yuting Deng [1], Yue Gao [2] and Changyi Yang [2]

[1] AECC Beijing Institute of Aeronautical Materials, Beijing 100095, China; lervly@sina.com (J.L.); ting_yudeng@163.com (Y.D.)
[2] Key Laboratory of Aerospace Advanced Materials and Performance of Ministry of Education, School of Materials Science and Engineering, Beihang University, Beijing 100191, China; by2101208@buaa.edu.cn (Y.G.); by2201154@buaa.edu.cn (C.Y.)
[3] AVIC Guizhou Anda Aviation Forging Co., Ltd., Anshun 561005, China; xchl0221@163.com
* Correspondence: zb2201102@buaa.edu.cn

Abstract: The microstructural stability and property evolution of high-temperature titanium alloys under long-term high-temperature conditions has been a critical scientific issue in the field of advanced titanium alloys. In this work, we systematically investigated the precipitation behavior of silicides and ordered α_2 phase, which are closely related to the microstructural stability of Ti65 high-temperature alloy, during thermal exposure at 650 °C for different periods of time. Furthermore, the effects of thermal exposure on mechanical properties were evaluated using room temperature and high temperature tensile tests, and subsequently, the correlation between the microstructural thermal stability and the mechanical characteristics was discussed. The results reveal that (Ti, Zr)$_6$Si$_3$ silicides initially precipitate within the residual β film and then start to precipitate in the α platelet. A large number of fine spherical α_2 precipitates were formed inside the α platelet after a short thermal exposure. The number density of ordered α_2 decreased significantly after 1000 h due to Ostwald ripening. The precipitation of silicides and ordered α_2 phases during thermal exposure improves the tensile strength but deteriorates the ductility, and the room-temperature ductility is slightly restored due to α_2 ripening after long-time thermal exposure. Ti65 high-temperature titanium alloy consistently maintains favorable room-temperature tensile properties throughout long-term thermal exposure.

Keywords: high-temperature titanium alloy; thermal exposure; silicide; ordered α_2 phase; mechanical properties

Citation: Li, J.; Jiang, W.; Xia, C.; Deng, Y.; Gao, Y.; Yang, C. Microstructural Evolution and Subsequent Mechanical Properties of Ti65 Titanium Alloy during Long-Term Thermal Exposure. *Metals* **2024**, *14*, 854. https://doi.org/10.3390/met14080854

Academic Editor: Frank Czerwinski

Received: 4 June 2024
Revised: 30 June 2024
Accepted: 15 July 2024
Published: 25 July 2024

1. Introduction

Titanium alloy has been widely used in aviation and aerospace fields because of its low density, high specific strength, excellent corrosion resistance, good high temperature resistance, and other advantages [1,2]. At present, the amount of titanium used in the aerospace industry accounts for more than half of the world's titanium market [3]. High-temperature titanium alloy exhibits excellent high-temperature performance and can partially replace the traditional materials used in aero-engines, such as steel or nickel-based high-temperature alloys. They have also been widely used in manufacturing blades, blisks, and casing in aero-engines in order to achieve the goal of reducing the weight of the engine to enhance the thrust-to-weight ratio and fuel efficiency [4,5]. High-temperature titanium alloys have become the key structural materials for hotend components of modern aero-engines. At present, commercial high-temperature titanium alloys are mainly near-α high-temperature titanium alloys based on the Ti–Al–Sn–Zr–Mo–Si alloy system, such as IMI834, Ti600, Ti6242S, etc. [6–8]. However, due to their microstructural stability deficiencies, long-term exposure to high temperatures may lead to room temperature plasticity, toughness, and fatigue performance degradation, conveying great risks to the long-term service of the components [9]. Therefore, the thermal stability of high-temperature titanium alloys is the focus of research in the field of advanced titanium alloys.

To further enhance the service temperature and high-temperature performance of high-temperature titanium alloys, researchers have introduced additional alloying elements such as Nb, Ta, W, and C into the Ti–Al–Sn–Zr–Mo–Si alloy system [10–13]. Currently, high-temperature titanium alloys contain nearly 10 alloying elements. Due to the complex alloying, the long-term high-temperature environment will lead to changes in the internal microstructure of the alloy, mainly including the precipitation of the coherent ordered α_2-Ti_3Al phase and the noncoherent silicide phase [9,14–16]. A large number of α_2-Ti_3Al phases precipitate via ordered transformations during the thermal exposure. While the precipitation of the α_2 phase can strengthen the interface configuration and lattice mismatch, it leads to a significant deterioration of ductility and toughness. It has been reported that the effect of ductility of near-α titanium alloys due to α_2-Ti3Al was found to be influenced by the population, size, and shape of α_2-Ti_3Al particles [17,18]. Besides, in the process of thermal exposure, the solubility of Si in titanium alloys decreases, leading it to combine with elements such as Ti and Zr to form silicide precipitation. The precipitation of silicides at the grain boundaries and α/β interfaces can hinder the dislocation movement, yet the high number of silicides can cause a decrease in creep resistance and adversely affect thermal stability performance, which has been reported in the research on Ti60 alloy and Ti1100 [19–21].

The Ti65 alloy is designed and developed as a nearly α-type high-temperature titanium alloy intended for service at 600–650 °C. The high-temperature stability of the internal microstructure of the alloy is an important indicator for evaluating its long-term stability and reliability. The precipitation and growth of the ordered α_2 phase and silicides are the main factors affecting the thermal stability of nearly α-type high-temperature titanium alloys. Therefore, in this study, TEM and other characterization methods were used to observe the precipitation behaviors of silicides and the ordered α_2 phases of Ti65 alloy with typical lamellar organization during long-term thermal exposure at 650 °C. The present investigation is focused on the microstructural thermal stability of the alloy and its influence on the mechanical properties.

2. Materials and Methods

The material used in this study was a high-temperature Ti65 alloy of the Ti–Al–Zr–Mo–Nb–Ta–Si–W system. The β-transition temperature of the alloy was determined by metallography to be 1040 °C. The Ti65 forging was solution-treated above T_β for 30 min and then aged at 750 °C for 2 h, followed by air cooling. A typical lamellar microstructure was finally obtained as the initial state.

To investigate the effect of thermal exposure on the microstructure and mechanical properties of Ti65 alloy with an initial lamellar microstructure, the solution and aging-treated Ti65 forgings were cut into thermal-exposed specimens with dimensions of 100 mm (length) × 15 mm (width) × 15 mm (thickness) using a WGM4 (Suzhou Posittec CNC Equipment Co., Ltd., Suzhou, China) wire-cutting machine. In order to avoid oxidation of the samples during thermal exposure, the samples were vacuum-sealed and protected with argon gas. The samples underwent thermal exposure experiments at 650 °C using a KSL-1750 box furnace (Hefei Kejing materials technology Co., Ltd., Hefei, China) for durations of 8 h, 100 h, 500 h, and 1000 h, followed by air-cooling to room temperature. The initial state sample and the thermal exposure sample were machined into a standard "dog bone" type tensile specimen, with a gauge length of 25 mm and a diameter of 5 mm. Uniaxial tensile tests were performed on an INSTRON 1195 testing machine at a strain rate of 10^{-3} s^{-1} at room temperature, according to standard GB/T 228.1-2010 [22]. High-temperature tensile tests were performed on an INSTRON 4507 testing machine equipped with a laser extensometer and a resistance heating furnace at a strain rate of 10^{-3} s^{-1} at

650 °C, according to standard GB/T 4338-2006 [23]. Three samples at each state were tested to ensure the data reproducibility, and the final results were averaged.

The evolution of the microstructure and composition was observed using a scanning electron microscope (SEM, FEI nova navo SEM450, Thermo FisherScientific Inc., Waltham, MA, USA) simultaneously equipped with an energy dispersive spectrometer (EDS, Inca E350 Oxford Instruments, Abingdon, UK). The SEM samples were ground by a series of SiC abrasive papers, mechanically polished, and then etched with standard Kroll's reagent (10 mL HF + 30 mL HNO_3 + 70 mL H_2O). The detailed microstructures were characterized using a Tecnal G2 F20 Transmission electron microscope (TEM, Thermo FisherScientific, Waltham Inc., Waltham, MA, USA) at a voltage of 200 kV. TEM samples with a thickness of 0.3 mm were prepared by cutting and mechanical grounding to 40–50 μm, followed by jet polishing at −20 °C using an MTP-1A double-jet polisher. The electrolyte formulation was 6% perchloric acid + 35% n-butanol + 59% methanol.

3. Results and Discussion

3.1. Initial Structure

The SEM morphology and EDS analysis results of the initial lamellar microstructure of the Ti65 alloy are shown in Figure 1a,b. After solid solution and aging heat treatment, the α phase transformed from the β phase exhibits a lamellar morphology. A distinct and continuous α phase precipitated at the original β grain boundary (α_G), as indicated by the green dashed line in Figure 1a, with a width of approximately 7 μm. The lamellar α_S and residual β film are distributed inside the course β grains, the α_S are fine in size with a width of about 2 μm, and the lamellar α_S of the same orientation form the α colonies (as shown in the orange dashed box in Figure 1a). The EDS analysis results show little difference in the distribution of elements within α_G and α_S, mainly due to the fact that both the α_G and α_S phases nucleate and grow during cooling from the β-phase region, with redistribution of elements occurring during subsequent aging treatments. Therefore, α_G and α_S only show differences in morphology, and the distribution of alloying elements is relatively uniform.

The initial lamellae microstructure was further observed using TEM, with the results depicted in Figure 1c–f. From the bright-field (BF) TEM in Figure 1c, an ellipsoidal precipitation phase can be observed between the α_S platelets, which grows along the lamellar interface and extends towards the α_S substrate, with a size of approximately 50 nm. The precipitation phase was subjected to analysis using EDS and selected area electron diffraction (SAED), as illustrated in Figure 1d,e. By calculating the lattice parameters and comparing them with those in the literature, it was determined that the precipitated phase is $(Ti, Zr)_6Si_3$-type silicide [24,25]. High-temperature titanium alloys improve the creep properties of the alloy by adding a small amount of Si, typically ranging from 0.1 to 0.5 wt%, in the high temperature Ti alloys developed. Since Si is a rapid eutectoid and a strong β stabilized element, the solid solubility is 3.0% in β-Ti, compared to just 0.45% in α-Ti [21,26,27]. The Ti65 alloy contains 0.4 wt% of Si, which tends to segregate to the β-phase during the solid solution treatment cooling process. During the aging process, the residual β film caused the eutectoid reaction to produce silicide. As a result, the precipitation of Ti_6Si_3-type silicide was observed between the α platelets in the initial lamellae microstructure after solid solution and aging treatment.

The selected area electron diffraction (SAED) pattern, taken from the $[\bar{1}102]_\alpha$ zone axis of the α-Ti platelet, is shown in Figure 1f. In addition to displaying HCP structural α-Ti diffraction spots on the α-Ti platelet, the pattern also exhibits faint superlattice diffraction spots, indicating that the α_2 phase has been formed in the α-Ti platelet of the Ti65 alloy after solid solution and aging heat treatment. A related dark field image acquired from an α_2 reflection, viewed along the $[\bar{1}102]_\alpha$ direction, as shown in Figure 1g, revealed a uniform distribution, with fine-sized spherical α_2 phases with sizes less than 5 nm.

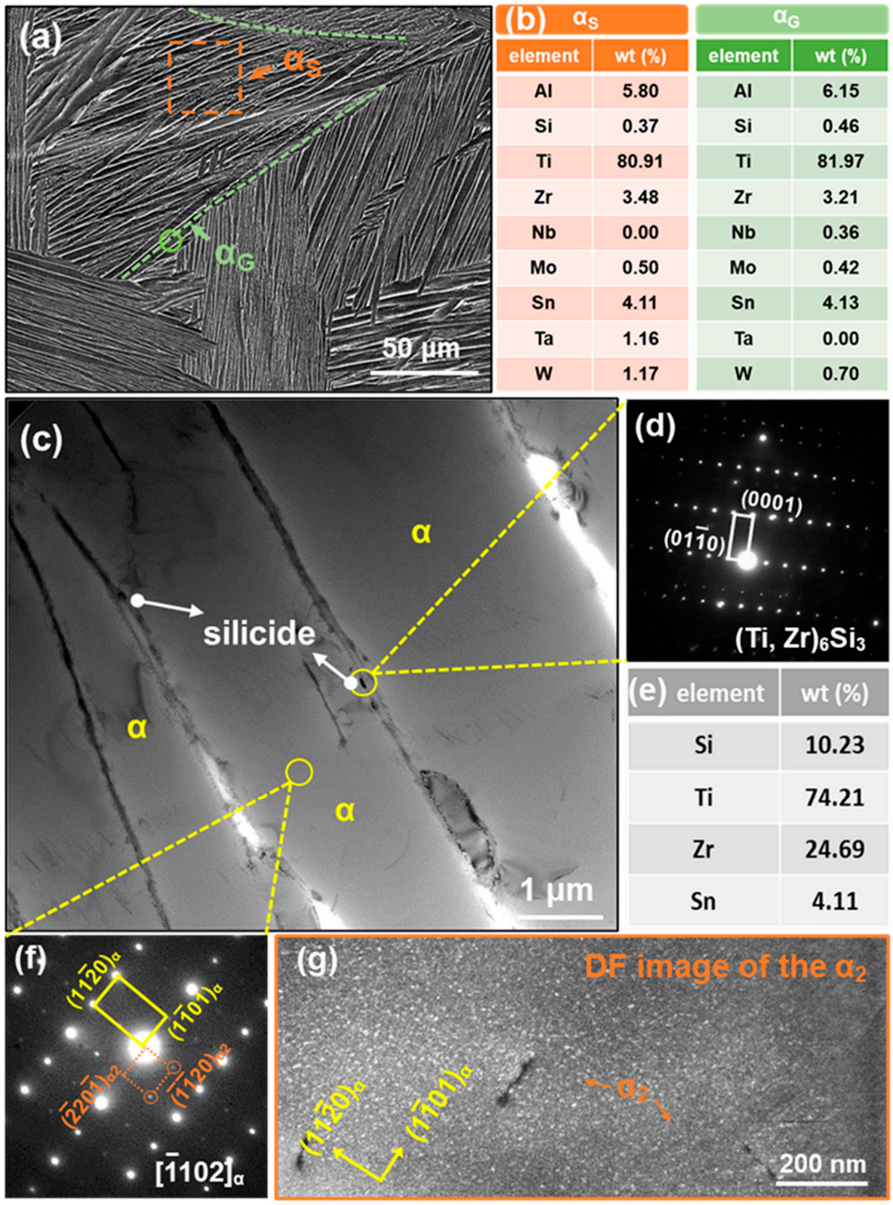

Figure 1. Microstructure observation of Ti65 alloy in the initial condition: (**a**) SEM image; (**b**) EDS results of α_G and α_S phases; (**c**) TEM bright-field image; (**d**) SAED pattern of silicide; (**e**) EDS results for silicide; (**f**) SAED pattern of α platelet; (**g**) TEM dark-field image of α_2 phase.

3.2. Microstructural Evolution

The microstructural evolution of the Ti65 alloy lamellar structure with prolonged thermal exposure time is shown in Figure 2a–d. After thermal exposure, the morphology of the lamellar structure showed no significant changes, still consisting of a lamellar transformed β structure(β_t) and a grain boundary α(α_G) distributed continuously along the grain boundaries. In comparison to the original morphology of the lamellar microstructure depicted in Figure 1a, the α_G gradually coarsens with prolonged thermal exposure time. Additionally, the initially elongated α_G begins to extend towards the lamellar β_t, forming a blocky and continuous α_G. The interface between neighboring lamellae α becomes increasingly blurred with prolonged thermal exposure, possibly due to the decomposition of residual β film during the thermal exposure process, which leads to the migration of the α/α interface.

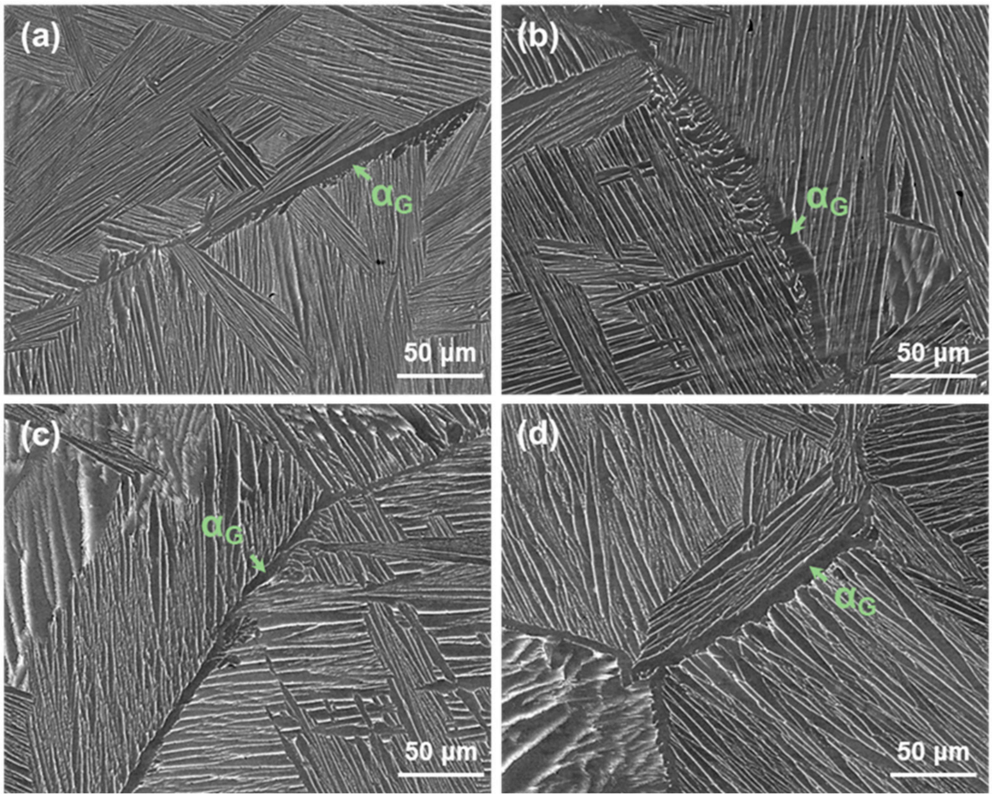

Figure 2. SEM images showing the change in the lamellar structure morphology with exposure times of (**a**) 8 h, (**b**) 100 h, (**c**) 500 h, and (**d**) 1000 h.

The EDS elemental analysis of the grain boundary α-phase and secondary α-phase of the lamellar microstructure after thermal exposure was conducted, as depicted in Figure 3a,b. It can be seen that for the strong α-stabilized element Al, the elemental content of Al in the grain boundary α-phase is slightly higher than that in the intracrystalline secondary α-phase. With the prolongation of thermal exposure, only the β-stabilized elements Zr, Ta, and W show an increasing trend in the grain boundary α and intracrystalline secondary α-phases. The thermal exposure process mainly occurs with the migration of elements in the residual β-phase into the α-phase with increasing time.

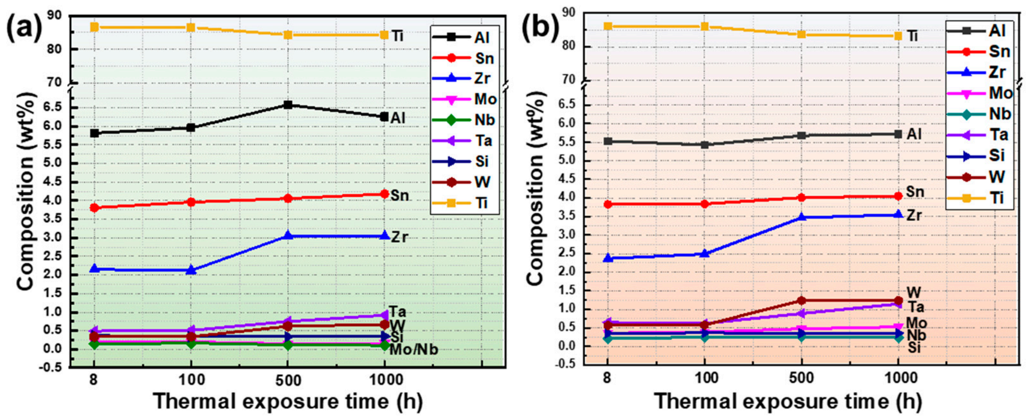

Figure 3. Elemental changes in the lamellar microstructure of Ti65 alloy under different thermal exposure times: (**a**) grain boundary $\alpha(\alpha_G)$; (**b**) lamellar secondary $\alpha(\alpha_S)$.

3.3. Silicide Precipitation

The precipitation of silicide at different thermal exposure times was observed using TEM. Figure 4a–d shows the TEM bright field images of samples that were thermally exposed for different times at 650 °C, taken from the same zone axis $[2\overline{1}\overline{1}0]_{\alpha}$. The inset in Figure 4a–d provides an enlarged view of the silicides. From the Figure 4a–d, it can be seen that the number and size of silicides increased significantly with the increase in thermal exposure time. The silicides after thermal exposure were identified as $(Ti, Zr)_6Si_3$ -type silicides, based on the SAED pattern, as shown in Figure 4e.

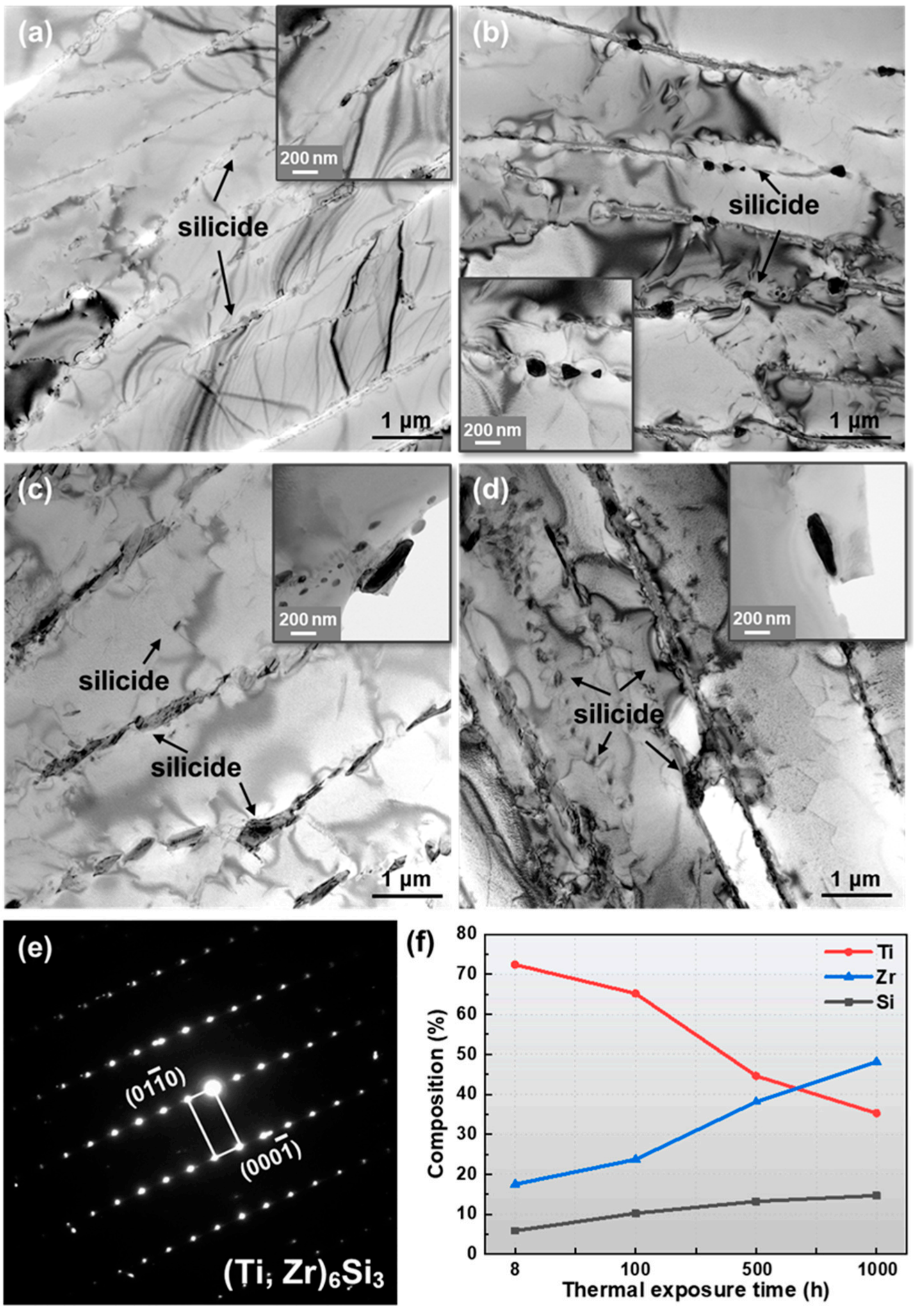

Figure 4. TEM bright field images of Ti65 alloy after thermal exposure at 650 °C for (**a**) 8 h, (**b**) 100 h, (**c**) 500 h, and (**d**) 1000 h; (**e**) SAED pattern of silicide after thermal exposures; (**f**) silicide composition with thermal exposure time.

When thermally exposed for 8 h (Figure 4a), the silicides between the α platelets exhibit slight coarsening compared to that of the initial state (Figure 1c), with a size of approximately 60 nm, due to the fact that the silicon atoms dissolved into the residual β film are still supersaturated. Additionally, many smaller-sized silicides nucleated and precipitated in the residual β film. When the thermal exposure time was extended to 500 h, the size of the initially precipitated silicides between the α platelets had coarsened to about 250 nm. As the thermal exposure time is further extended, the size and number of silicides precipitated from the residual β film between the α platelets gradually tend to stabilize, with little difference observed in the size and number of silicides between thermal exposure times of 1000 h and 500 h, as shown in Figure 4c,d.

It is noted that the precipitation of silicides was observed within the α platelets, as shown in Figure 4c. This is primarily attributed to the decrease in silicide solubility within the α matrix during thermal exposure at 650 °C. As the thermal exposure reaches 500 h, the excess silicide within the α matrix preferentially induces the precipitation and growth of silicides within the matrix at dislocations, along with other defects [15,28,29]. The nucleation and growth of silicides within the α platelets continue with increasing thermal exposure time, as illustrated in Figure 4d. Therefore, during long-term thermal exposure at 650 °C, the solid solubility of Si in both the α platelets and residual β film decreases, at which time the residual β film will decompose to form silicides, while excess Si within the lamellar α platelets causes the precipitation and growth of silicides within the matrix. The above results indicate that there is no precipitation of new types of silicides after long-term thermal exposure, but the treatment leads primarily to the precipitation and growth of $(Ti, Zr)_6Si_3$-type silicides. Moreover, the precipitation location, quantity, and density change with the prolongation of thermal exposure time.

The composition of the silicides was analyzed during thermal exposure time using EDS, as shown in Figure 4f. For the $(Ti, Zr)_6Si_3$ type silicides, the primary constituents identified were Ti, Zr, and Si. However, as the thermal exposure time is extended, there is a noticeable change in the content of the main components. As depicted in Figure 4f, the Ti element content in the silicide gradually decreases, whereas the Zr element content gradually increases. It has been reported that although Zr and Ti have the same chemical valence, Zr displaces part of Ti, and through this displacement, it can reduce the high strain energy caused by the structural mismatch between the α-phase of the HCP structure and the silicide, which in turn reduces the nucleation activation energy of the silicide [26,30–32]. Thus, the addition of Zr to high-temperature titanium alloys can refine the size of the silicides and promote their diffuse distribution. Combining the above results of TEM bright field images with EDS analysis, it can be inferred that the growth of silicides is controlled by the diffusion of the alloying elements. As the thermal exposure time extends, elemental diffusion reaches a sufficient level, resulting in a deceleration of both the precipitation and growth of silicides.

3.4. Ordered α_2 Precipitation

The ordered transformation of the α_2 phase was also observed using TEM. Figure 5a,b shows the SAED results of the α platelets of the specimen after thermal exposure at 650 °C for 1000 h, viewed along typical $[\bar{1}102]_\alpha$ and $[2\bar{1}\bar{1}0]_\alpha$ directions. Superlattice diffraction spots can be clearly observed, with their diffraction intensities markedly higher than those of the initial state, indicating the formation of ordered α_2 precipitation during the thermal exposure process. As shown in Figure 5a, the orientation relationship between the α- and α_2-phases is $[\bar{1}102]_\alpha//[\bar{1}104]_{\alpha 2}$ and $(11\bar{2}0)_\alpha//(\bar{1}\bar{1}20)_{\alpha 2}$.

In order to further characterize the precipitation behavior of the α_2 ordered precipitation within the α platelets considering thermal exposure time, dark field images of the α_2 phase along the $[\bar{1}102]_\alpha$ incidence direction were observed, as shown in Figure 6a–d. It can be observed that after 8 h of thermal exposure, a large number of fine-sized spherical α_2 phases have been uniformly precipitated from the α platelets, with an increase in size to 8 nm compared to that of the initial state (Figure 6a). After 100 h of thermal exposure, the ordered transformation is continued, and the ordered α_2 phase grows to 12 nm, while the morphology does not change (Figure 6b). After 500 h of thermal exposure, the α_2 phase was further coarsened, and the average size increased to about 15 nm, as shown in Figure 6c. After a long-term thermal exposure of 1000 h (Figure 6d), the size of the α_2

phase is basically stable, without further coarsening, and the morphology of the ordered α_2 phase also remains spherical.

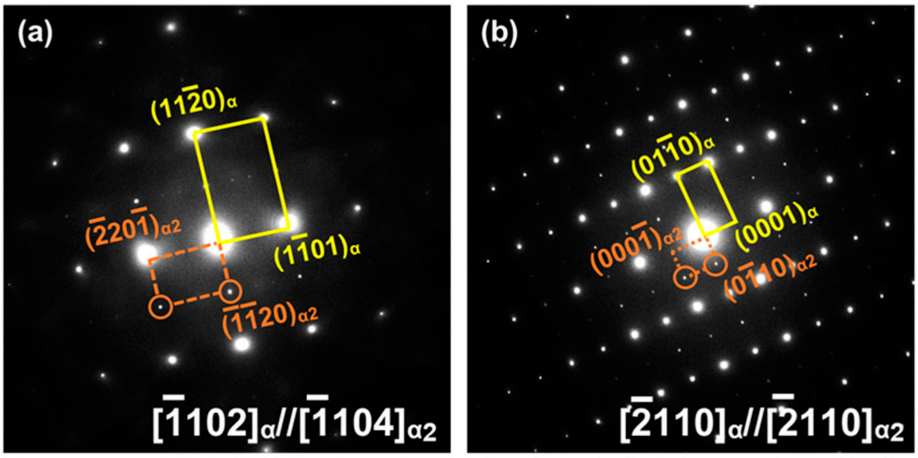

Figure 5. Typical SAED patterns of Ti65 alloy after thermal exposure with incident direction (**a**) $[\bar{1}102]_{\alpha}//[\bar{1}104]_{\alpha2}$ and (**b**) $[\bar{2}110]_{\alpha}//[\bar{2}110]_{\alpha2}$, showing superlattice reflections from α_2-phase.

It should be noted that after 500 h of thermal exposure, a declining trend in the number of α_2 precipitated phases can be observed, and when 1000 h is reached, the number of α_2 phases decreases significantly. With the increase in thermal exposure time, the α_2 phase will undergo Ostwald ripening, where the small-sized α_2 precipitates gradually dissolve and disappear, while the large-sized precipitates begin to coarsen [33–36]. Ostwald ripening is a phenomenon commonly observed in solid solutions. This process involves the dissolution of particles smaller than a critical size, followed by the transfer of mass to particles larger than this critical size [35,37,38]. Therefore, a significantly decrease in the number density of α_2 phase can be observed after 1000 h of thermal exposure.

3.5. Mechanical Property

In order to investigate the effect of thermal exposure on the mechanical properties of Ti65 alloy, room temperature and high temperature tensile tests were performed. The room temperature and high temperature tensile properties of Ti65 alloy with an initial lamellar microstructure after thermal exposure at 650 °C for different times are shown in Figure 7a,b. For the room temperature tensile properties (Figure 7a), both the yield strength (YS) and ultimate tensile strength (UTS) increased significantly after 8 h of thermal exposure, with a slight decrease in elongation (EI). Upon further exposure up to 100 h, UTS and YS reached the maximum. When thermal exposure reached 500 h, the strength stabilized and the elongation decreased to a minimum. Following 1000 h of thermal exposure, the strength and elongation remained stable and still exhibited good room temperature tensile properties. For the high-temperature (650 °C) tensile properties (Figure 7b), the yield strength and ultimate tensile strength remained relatively stable with increasing thermal exposure time. However, the elongation reached its maximum after 100 h of thermal exposure and then decreased significantly, dropping to 9.3% after 1000 h. The specimens exposed to 100 h of treatment exhibited the best high-temperature performance.

Several studies have pointed out that microstructural changes induced by thermal exposure have a significant effect on the mechanical properties of titanium alloys [39–43]. The above results also indicate that the alterations in the precipitation behavior of silicides and α_2 ordered phases are closely related to the changes in the tensile properties of the Ti65 alloys. During thermal exposure, the formation of α_2 ordered phases and silicides can impede dislocation movement through a cutting mechanism [44,45], resulting in the increase in alloy strength. The presence of a large number of α_2 ordered phases changes the dislocation slip mode from dislocation cross-slip to planar dislocation slip [46]. Therefore, the precipitation of α_2 ordered phase reduces the ductility. However, with prolonged thermal exposure, the α_2 ordered phase undergoes coarsening, and the number density decreases, which increases the mean free range of dislocation slip [47]. Hence, the ductility recovered slightly after long-term thermal exposure.

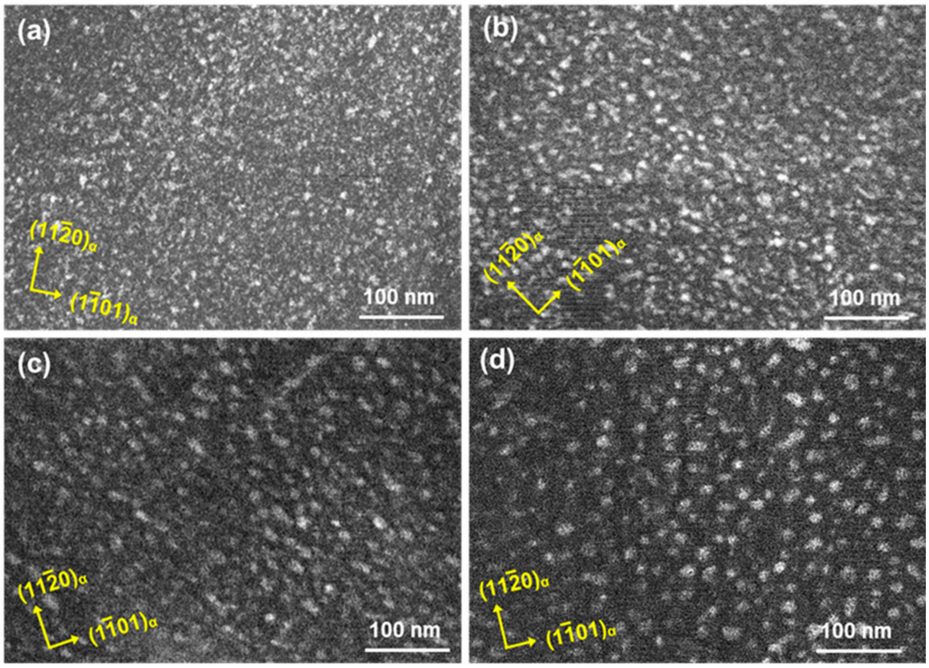

Figure 6. Dark field image morphology of Ti65 alloy along the $[\bar{1}102]_\alpha$ incidence direction after thermal exposure for different times: (**a**) 8 h, (**b**) 100 h, (**c**) 500 h, and (**d**) 1000 h.

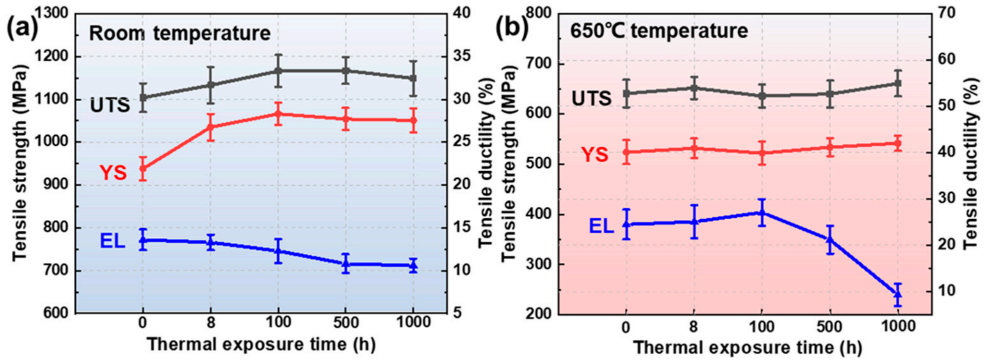

Figure 7. The variation in tensile properties at (**a**) room temperature and (**b**) 650 °C of Ti65 alloys with prolonged thermal exposure.

For high-temperature (650 °C) tensile properties, the tensile ductility shows an unexpected sharp decrease after 500 h of thermal exposure. This can be attributed to two potential reasons. On the one hand, due to the long-term thermal exposure, the silicides at the interface undergo significant coarsening, which causes stress concentration and prompts the initiation of microcracks between the interface of the silicide and the matrix, resulting in intergranular failure. On the other hand, after 500 h of thermal exposure at 650 °C, silicide phase has been precipitated within the α platelets of Ti65 alloy, and if the tensile test is continued at 650 °C, a large number of fine silicides will continue to be precipitated inside the α platelets in the process of tensile deformation. The precipitated silicides within the α platelets will impede dislocation motion and make local deformation more difficult, which decreases the plasticity.

4. Conclusions

In this work, the microstructure thermal stability and mechanical properties of Ti65 high-temperature titanium alloy under thermal exposure conditions at 650 °C are systematically discussed. The precipitation behaviors of silicides and α_2 ordered phases during thermal exposure are analyzed in detail by using TEM technique. The main conclusions are as follows:

1. After solid solution and aging heat treatment of Ti65 alloy, the initial lamellae microstructure contains precipitated (Ti, Zr)$_6$Si$_3$ silicides at the α/β phase boundary, as well as diffusely precipitated α_2 ordered phases within the matrix. The dual-phase precipitation strengthening resulted in the initial state Ti65 alloy exhibiting favorable room temperature properties (YS = 928 MPa, UTS = 1083 MPa, EI = 13.6%), as well as good high-temperature properties (YS = 524 MPa, UTS = 641 MPa, EI = 24.5%).
2. (Ti, Zr)$_6$Si$_3$ silicides initially precipitate in the residual β-film between the α platelets, and the size and density increase with prolonged thermal exposure. After 500 h, the size and density of silicides at the α/β interface tend to stabilize. Simultaneously, the precipitation location of the elliptical silicides changes, initiating precipitation within the α platelets, with the size and quantity continuing to increase with the extension of the thermal exposure time. The precipitation and growth of silicides are controlled by the diffusion of the alloying elements.
3. After thermal exposure at 650 °C, a large number of spherical α_2 ordered phases were precipitated within the α matrix. The α_2 ordered phases remained spherical but exhibited considerable coarsening as the thermal exposure time increased. Following 1000 h of thermal exposure, the α_2 phase underwent Oswald ripening, resulting in a decrease in number density.
4. The effect of thermal exposure on the mechanical properties of Ti65 alloy is closely related to the precipitation behavior of silicides and α_2 ordered phase. With the increase in thermal exposure time, the precipitation of silicides and α_2 ordered phases increases the room temperature strength and decreases the ductility. After prolonged thermal exposure, the room temperature ductility is slightly restored due to the decrease in α_2 phase density within the α matrix.

Author Contributions: Conceptualization, J.L., W.J. and C.Y.; methodology, J.L., C.X. and Y.D.; software, J.L. and C.X.; validation, C.X., Y.G., C.Y. and Y.D.; formal analysis, J.L. and W.J.; investigation, J.L. and W.J.; resources, C.Y. and Y.D.; data curation, J.L., Y.G. and C.Y.; writing—original draft preparation, J.L., C.X. and Y.D.; writing—review and editing, W.J., Y.G. and C.Y.; visualization, Y.G. and C.Y.; supervision, W.J.; project administration, J.L.; funding acquisition, J.L. All authors have read and agreed to the published version of the manuscript.

Funding: This research was funded by the National Science and Technology Major Project (J2019-VI-0005-0119) & the National Science and Technology Major Project (J2019-VI-0012-0126).

Data Availability Statement: The data presented in this study are available on request from the corresponding author. The data are not publicly available due to privacy concerns.

Conflicts of Interest: Author Chunlin Xia was employed by the company AVIC Guizhou Anda Aviation Forging Co., Ltd. The remaining authors declare that the research was conducted in the absence of any commercial or financial relationships that could be construed as a potential conflict of interest.

References

1. Banerjee, D.; Williams, J. Perspectives on titanium science and technology. *Acta Mater.* **2013**, *61*, 844–879. [CrossRef]
2. Boyer, R.R. An overview on the use of titanium in the aerospace industry. *Mater. Sci. Eng. A* **1996**, *213*, 103–114. [CrossRef]
3. Zhao, Q.Y.; Sun, Q.Y.; Xin, S.W.; Chen, Y.N.; Wu, C.; Wang, H.; Xu, J.W.; Wan, M.P.; Zeng, W.D.; Zhao, Y.Q. High-strength titanium alloys for aerospace engineering applications: A review on melting-forging process. *Mater. Sci. Eng. A* **2022**, *845*, 143260. [CrossRef]
4. Gogia, A. High-temperature titanium alloys. *Def. Sci. J.* **2005**, *55*, 149–173. [CrossRef]

5. Cai, J.M.; Mi, G.B.; Gao, F.; Huang, H.; Cao, J.X.; Huang, X.; Cao, C.X. Research and development of some advanced high temperature titanium alloys for aero-engine. *J. Mater. Eng.* **2016**, *44*, 1–10.
6. Es-Souni, M. Creep deformation behavior of three high-temperature near α-Ti alloys: IMI 834, IMI 829, and IMI 685. *Metall. Mater. Trans. A* **2001**, *32*, 285–293. [CrossRef]
7. Es-Souni, M. Primary, secondary and anelastic creep of a high temperature near α-Ti alloy Ti6242Si. *Mater. Charact.* **2000**, *45*, 153–164. [CrossRef]
8. Niu, Y.; Hou, H.L.; Li, M.Q.; Li, Z.Q. High temperature deformation behavior of a near alpha Ti600 titanium alloy. *Mater. Sci. Eng. A* **2008**, *492*, 24–28. [CrossRef]
9. Woodfield, A.; Postans, P.; Loretto, M.; Smallman, R. The effect of long-term high temperature exposure on the structure and properties of the titanium alloy Ti-5331S. *Acta Metall.* **1988**, *36*, 507–515. [CrossRef]
10. Zhang, W.J.; Song, X.Y.; Hui, S.X.; Ye, W.J.; Wang, Y.L.; Wang, W.Q. Tensile behavior at 700 °C in Ti–Al–Sn–Zr–Mo–Nb–W–Si alloy with a bi-modal microstructure. *Mater. Sci. Eng. A* **2014**, *595*, 159–164. [CrossRef]
11. Li, J.; Xu, Y.Q.; Xiao, W.L.; Ma, C.L.; Huang, X. Development of Ti-Al-Ta-Nb-(Re) near-α high temperature titanium alloy: Microstructure, thermal stability and mechanical properties. *J. Mater. Sci. Technol.* **2022**, *109*, 1–11. [CrossRef]
12. Zhang, S.Z.; Li, G.P.; Wang, Q.; Liu, Y.Y.; Yang, R. Effect of carbon on upper (α + β) phase field of Ti-5.6 Al-4.8 Sn-2.0 Zr-1Mo-0.34 Si-0.7 Nd titanium alloy. *Mater. Sci. J.* **2013**, *20*, 167–172.
13. Ma, X.Z.; Chen, Z.Y.; Xiang, Z.L.; Zhang, S.W.; Liu, Y.Y.; Ding, X.X. Influence of quenching plus aging on microstructures and mechanical properties evolutions for Ti-Al-Sn-Zr-Mo-Si-Nb-Ta-Er-C near-α high temperature titanium alloys. *Mater. Today Commun.* **2024**, *38*, 108457. [CrossRef]
14. Koike, J.; Egashira, K.; Maruyama, K.; Oikawa, H. High temperature strength of α TiAl alloys with a locally ordered structure. *Mater. Sci. Eng. A* **1996**, *213*, 98–102. [CrossRef]
15. Yue, K.; Liu, J.; Zhang, H.; Yu, H.; Song, Y.; Hu, Q.; Wang, Q.; Yang, R. Precipitates and alloying elements distribution in near α titanium alloy Ti65. *J. Mater. Sci. Technol.* **2020**, *36*, 91–96. [CrossRef]
16. Liu, X.H.; Zhang, X.Y.; Du, Y.X.; Li, S.Q.; Chen, H.S.; Li, K.E.; Zhao, D.X.; Chen, W. Insights into microstructural stability and embrittlement of TC25 high temperature titanium alloy subjected to thermal exposure. *Mater. Charact.* **2024**, *210*, 113820. [CrossRef]
17. Sun, F.; Li, J.; Kou, H.; Tang, B.; Cai, J. Nano-precipitation and tensile properties of Ti60 alloy after exposure at 550 °C and 650 °C. *Mater. Sci. Eng. A* **2015**, *626*, 247–253. [CrossRef]
18. Zhang, J.; Li, D. Preferred precipitation of ordered α_2 phase at dislocations and boundaries in near-α titanium alloys. *Mater. Sci. Eng. A* **2003**, *341*, 229–235. [CrossRef]
19. Ramachandra, C.; Singh, V. Silicide precipitation in alloy Ti-6Al-5Zr-0.5Mo-0.25Si. *Metall. Trans. A* **1982**, *13*, 771–775. [CrossRef]
20. Zhong, X.Y.; Deng, T.S.; Xiao, W.L.; Liu, X.C.; Liu, Z.; Yang, Y.C.; Olanrewaju, A.O. Improving thermal stability and creep resistance by Sc addition in near-α high-temperature titanium alloy. *J. Mater. Sci. Technol.* **2024**, *183*, 1–11. [CrossRef]
21. Zhao, E.; Sun, S.C.; Zhang, Y. Recent advances in silicon containing high temperature titanium alloys. *J. Mater. Sci. Technol.* **2021**, *14*, 3029–3042. [CrossRef]
22. *GB/T 228.1-2010*; Metallic Materials-Tensile Testing-Part 1: Method of Test at Room Temperature. China Standards Press: Beijing, China, 2010.
23. *GB/T 4338-2006*; Metallic Materials—Tensile Testing at Elevated Temperature. China Standards Press: Beijing, China, 2006.
24. Singh, A.; Ramachandra, C. Characterization of silicides in high-temperature titanium alloys. *J. Mater. Sci.* **1997**, *32*, 229–234. [CrossRef]
25. Sun, S.; Zhao, E.; Hu, C.; An, Y.; Chen, W. Precipitation behavior of silicide and synergetic strengthening mechanisms in TiB-reinforced high-temperature titanium matrix composites during multi-directional forging. *J. Alloys Compd.* **2021**, *867*, 159051. [CrossRef]
26. Flower, H.; Swann, P.; West, D. Silicide precipitation in the Ti-Zr-Al-Si system. *Metall. Mater. Trans. B* **1971**, *2*, 3289–3297. [CrossRef]
27. Pilchak, A.; Porter, W.; John, R. Room temperature fracture processes of a near-α titanium alloy following elevated temperature exposure. *J. Mater. Sci.* **2012**, *47*, 7235–7253. [CrossRef]
28. Zhao, D.; Fan, J.K.; Zhang, Z.X.; Wang, J.; Wang, Q.J.; Chen, Z.Y.; Tang, B.; Kou, H.C.; Li, J.S. Influence of α+β solution treatments on Ti65 ultrathin sheets: Silicide precipitation, mechanical behaviour and novel {101¯1} twinning system. *Trans. Nonferrous Metals Soc. China* **2023**, *33*, 1098–1113. [CrossRef]
29. Li, J.; Cai, J.M.; Xu, Y.Q.; Xiao, W.L.; Huang, X.; Ma, C.L. Influences of thermal exposure on the microstructural evolution and subsequent mechanical properties of a near-α high temperature titanium alloy. *Mater. Sci. Eng. A* **2020**, *774*, 138934. [CrossRef]
30. Varlioglu, M.; Nash, P. The effect of increased zirconium content on the microstructure and mechanical properties of Ti-1100 alloy. *Light Met. Age* **2004**, *62*, 32–35.
31. Fu, B.; Wang, H.; Zou, C.; Wei, Z. The influence of Zr content on microstructure and precipitation of silicide in as-cast near α titanium alloys. *Mater. Charact.* **2015**, *99*, 17–24. [CrossRef]
32. Mi, G.B.; Chen, H.; Li, P.J.; Cao, C.X. Mechanism of graphene oxide promoting silicide precipitation in high-temperature titanium alloy. *Mater. Today Commun.* **2023**, *37*, 106932. [CrossRef]

33. Radecka, A.; Coakley, J.; Vorontsov, V.; Martin, T.; Bagot, P.; Moody, M.; Rugg, D.; Dye, D. Precipitation of the ordered α2 phase in a near-α titanium alloy. *Scr. Mater.* **2016**, *117*, 81–85. [CrossRef]
34. Lunt, D.; Busolo, T.; Xu, X.; da Fonseca, J.Q.; Preuss, M. Effect of nanoscale α2 precipitation on strain localisation in a two-phase Ti-alloy. *Acta Mater.* **2017**, *129*, 72–82. [CrossRef]
35. Perez, M.; Dumont, M.; Acevedo-Reyes, D. Implementation of classical nucleation and growth theories for precipitation. *Acta Metall.* **2008**, *56*, 2119–2132. [CrossRef]
36. Youssef, S.S.; Zheng, X.D.; Huang, S.S.; Ma, Y.J.; Qi, M.; Zheng, S.J.; Lei, J.F.; Yang, R. Precipitation behavior of α2 phase and its influence on mechanical properties of binary Ti-8Al alloy. *J. Alloys Compd.* **2021**, *871*, 159577. [CrossRef]
37. Werz, T.; Baumann, M.; Wolfram, U.; Krill III, C.E. Particle tracking during Ostwald ripening using time-resolved laboratory X-ray microtomography. *Mater. Charact.* **2014**, *90*, 185–195. [CrossRef]
38. Hardy, S.C.; Voorhees, P.W. Ostwald ripening in a system with a high volume fraction of coarsening phase. *Metall. Mater. Trans. A* **1988**, *19*, 2713–2721. [CrossRef]
39. Jia, W.J.; Zeng, W.D.; Yu, H.Q. Effect of aging on the tensile properties and microstructures of a near-alpha titanium alloy. *Mater. Des.* **2014**, *58*, 108–115. [CrossRef]
40. Zhang, H.Z.; Lin, B.; Sun, Q.Q.; Liu, J.X.; Ning, B.; Wang, S. The mechanism for annealing-induced ductile to brittle transition in a high-temperature titanium alloy and its mitigation. *Mater. Sci. Eng. A* **2024**, *898*, 146370. [CrossRef]
41. Sun, J.F.; Lu, H.F.; Zhang, H.M.; Luo, K.Y.; Lu, J.Z. Effect of thermal exposure on microstructure and mechanical properties of Ti65 high-temperature titanium alloy deposited by laser direct energy deposition. *Mater. Sci. Eng. A* **2024**, *908*, 146757. [CrossRef]
42. Madsen, A.; Ghonem, H. Separating the effects of Ti3Al and silicide precipitates on the tensile and crack growth behavior at room temperature and 593 °C in a near-alpha titanium alloy. *J. Mater. Eng. Perform.* **1995**, *4*, 301–307. [CrossRef]
43. Lütjering, G.; Weissmann, S. Mechanical properties of age-hardened titanium-aluminum alloys. *Acta Metall.* **1970**, *18*, 785–795. [CrossRef]
44. Cai, J.M.; Huang, X.; Cao, C.X.; Ji-Min, M.A. Microstructural evolution of near-α titanium alloy during long-term high temperature exposure and its influence on thermal stability. *J. Aeronaut. Mater.* **2010**, *30*, 11–18.
45. Christoph, L.; Manfred, P. Influence of long-term annealing on tensile properties and fracture of near α-titanium alloy Ti-6Al-2.75Sn-4Zr-0.4Mo. *Metal. Mater. Trans. A* **1996**, *27*, 1709–1717.
46. Sastry, S.; Lipsitt, H. Ordering transformations and mechanical properties of Ti3Ai and Ti3Al-Nb alloys. *Metall. Trans. A* **1977**, *8*, 1543. [CrossRef]
47. Yu, T.; Wang, L.; Zhao, Y.Q.; Liu, Y. Effects of thermal exposure on cyclic deformation and fracture behavior of Ti600 titanium alloy. *Int. J. Fatigue* **2012**, *35*, 31–36. [CrossRef]